

锰基配位聚合物的简易合成、结构及其在葡萄糖电化学传感中的应用

赵璐 陈彤丹 王晗叶 李晨曦 李江*

(长安大学材料科学与工程学院, 西安 710064)

摘要: 利用刚性配体6-(3-吡啶基)间苯二甲酸(H_2PIAD), 制备了一种基于Mn(II)的配位聚合物 $\{[Mn(PIAD)(DMF)] \cdot H_2O\}_n$ (**1**)。采用后合成Ag纳米颗粒的策略制备了复合材料(Ag@**1**)以提高葡萄糖传感的电催化活性。在优化的外加电位下, 通过计时电流法评估了Ag@**1**修饰的玻碳电极(GCE)的电催化性能。配位聚合物**1**为在其表面的Ag纳米颗粒均匀分布提供了固定基质, 而且Ag@**1**传感器可以最大限度地发挥Ag与**1**结合对葡萄糖氧化的电催化协同效应。结果表明, Ag@**1**修饰的GCE对葡萄糖的检测性能良好, 检出限低($6.36 \mu\text{mol} \cdot \text{L}^{-1}$), 选择性和灵敏度好($166.71 \mu\text{A} \cdot \text{L} \cdot \text{mmol}^{-1} \cdot \text{cm}^{-2}$)。

关键词: 锰; 配位聚合物; Ag纳米颗粒; 葡萄糖传感

中图分类号: O614.71⁺1; O614.122

文献标识码: A

文章编号: 1001-4861(2021)11-2101-12

DOI: 10.11862/CJIC.2021.237

Mn-Based Coordination Polymer: Facile Synthesis, Structure and Application in Glucose Electrochemical Sensing

ZHAO Lu CHEN Tong-Dan WANG Han-Ye LI Chen-Xi LI Jiang*

(School of Materials Science and Engineering, Chang'an University, Xi'an 710064, China)

Abstract: Utilizing the rigid 6-(3-pyridyl) isophthalic acid (H_2PIAD) linker, one Mn(II)-based coordination polymer $\{[Mn(PIAD)(DMF)] \cdot H_2O\}_n$ (**1**) was prepared firstly. In order to improve the electrocatalytic activity of glucose sensing, a composite material (Ag@**1**) was prepared by the strategy of post synthesis of Ag nanoparticles (NPs). The electrocatalytic performance of the glassy carbon electrode (GCE) modified by Ag@**1** was evaluated by chronoamperometry method at the optimized application potential, and coordination polymer **1** provided a fixed substrate for the uniform distribution of Ag NPs on its surface. Ag@**1** sensor can maximize the electrocatalytic synergistic effect of the combination of Ag and **1** on glucose oxidation. The results reveal that modified GCE by Ag@**1** had good performance for the detection of glucose with low detection limit ($6.36 \mu\text{mol} \cdot \text{L}^{-1}$), good selectivity and sensitivity ($166.71 \mu\text{A} \cdot \text{L} \cdot \text{mmol}^{-1} \cdot \text{cm}^{-2}$). CCDC: 2080639.

Keywords: manganese; coordination polymer; Ag nanoparticles; glucose sensor

0 Introduction

Diabetes mellitus is deemed a complex, chronic illness and have become one of the biggest threats to human health^[1]. Therefore, it is urgent to accurately

monitor glucose levels for reducing the risk of its long-term complications. At present, much more ongoing and reliable glucose sensors are very important. The electrochemical biosensors depend mainly on the activity of enzymes, such as glucose oxidase (GODx)^[2-3].

收稿日期: 2021-06-08. 收修改稿日期: 2021-08-31.

国家自然科学基金(No.22008011)、长安大学中央高校基金(No.300102310109)和陕西省博士后基金(No.2018BSHGZZHQYXMZZ28)资助。

*通信联系人。E-mail: lijia@chd.edu.cn

However, due to its complex preparation, the activity of biosensors can be easily affected by temperature, pH value, humidity, and toxic chemicals^[4-7]. Also, most enzyme-based sensors involve complex immobilization steps of glucose oxidase, which increases the uncertainty of bio-sensing^[8-9]. Accordingly, non-enzymatic electrochemical sensors can be profitable in low-cost, structural simplicity and long-term stability^[10-11].

To date, coordination polymers (CPs), as an important type of nanomaterial, have received considerable attention under the context of electrochemistry recently^[12], such as electrochemical sensing^[13-16], electrocatalysis^[17-18], bio-imaging^[19], supercapacitors^[20-22], and fuel cell catalyst^[23]. Thanks to the advantages of CPs, such as high specific surface area, tunable structure, rich active sites and tailorable structure^[24], these prospective features stimulate that CPs as a carrier for the immobilization of specific functional nanomaterials. Although the application success of CPs in the non-enzymatic sensors^[25], CPs with poor conductivity cannot play a significant role in avoiding inherent defects when applied to electrochemical sensing^[26]. Therefore, it is worth to consideration combining other functional nanomaterials with CPs to form a hybrid material achieving highly efficient sensing. Metal (*e.g.*, Pt, Au, Ag) nanoparticles (NPs) could increase specific surface areas and enhance mass transport ability in electrochemical sensors. And the NPs are usually combined with other materials such as porous carbon^[27-29], metal organic frameworks^[30-32] and graphene^[33-36] used for electrochemical sensing to enhance their catalytic activity. Chang et al.^[37] developed a facile and clean method by using ascorbic acid as a mild reductant to synthesize Pt/graphene composites under the assistance of polyvinyl-pyrrolidone (PVP). Chen et al.^[38] synthesized Ni(SA)₂(H₂O)₄ CP and transformed it into porous NiO nanorods with excellent electrocatalytic properties. The porous NiO modified glassy carbon (*p*-NiO/GC) electrode showed a wide linear range (0.01-5 mmol·L⁻¹), which could be used for determination of glucose in human serum samples. Among various metal NPs, Ag NPs possess high conductivity and biocompatibility, which increases their demand in the field of

sensing^[39]. However, NPs usually have the phenomenon of agglomeration, decreasing the active site^[40]. In this investigation, Mn(II)-based CPs was introduced to provide the matrix for the uniform distribution of Ag NPs. Thus, Ag NPs can be considered as the metal of choice together with CPs to amplify the electrocatalytic activity for glucose oxidation.

Herein, employing ligand 6-(3-pyridyl) isophthalic acid (H₂PIAD), one novel CPs, namely {[Mn(PIAD)(DMF)]·H₂O}_{*n*} (**1**), was constructed from the ligand and Mn(II) ions in specific solvent systems. Notably, compound **1** was chosen as a substrate, and Ag NPs were deposited onto the surface of **1**. The obtained Ag@**1** was further used to modify glassy carbon electrode (GCE) to establish an electrochemical sensing platform for glucose detection. The modified Ag@**1**/GCE possessed a suitable sensing performance for the sensitivity, selectivity, good stability and low detection limit (6.36 μmol·L⁻¹).

1 Experimental

1.1 Preparation of {[Mn(PIAD)(DMF)]·H₂O}_{*n*} (**1**)

A mixture containing MnCl₂·4H₂O (0.013 5 g, 0.068 mmol), 6-(3-pyridyl) isophthalic acid (0.019 5 g, 0.08 mmol), deionized water (1.0 mL), *N,N*-dimethylformamide (DMF, 3.0 mL) was ultrasonic mixing for 10 min, and transferred to autoclave and heated at 105 °C for three days. After cooling, faint yellow crystals were collected by filtration and dried at 40 °C for 4 h. Yield: 68% based on Mn. Anal. Calcd. for C₁₆H₁₆MnN₂O₆(%): C, 49.62; H, 4.16; N, 7.23. Found(%): C, 50.53; H, 4.24; N, 7.18. FT-IR (KBr, cm⁻¹): 3 414(w), 3 069(w), 1 580(s), 1 388(s), 1 171(m), 1 097(w), 1 036(m), 1 012(m), 924(m), 860(m), 821(s), 783(s), 763(m), 735(m), 706(s), 688(s), 659(m), 647(m), 621(m), 542(m), 474(m).

1.2 Preparation of Ag@**1**

Ag@**1** was synthesized based on a modified reported method^[41]. Compound **1** (50 mg) was added to 10 mL H₂O/DMF solution (1: 3, *V/V*) containing AgNO₃ (1 mmol·L⁻¹) and stirred overnight. Then the collected suspension was dispersed in 10 mL H₂O/DMF solvent (1: 3, *V/V*), followed by rapidly adding 5 mL of the

same mixed solvents containing NaBH_4 (0.1 mmol). The obtained sample was centrifuged and washed with ethanol five times.

1.3 Preparation of Ag@1 modified electrode

The glucose sensors as-fabricated by Mn(II)-based CPs (**1**) was assembled on the surface of the electrode to form a Nafion/Mn(II)-based CPs sensor film. Before modifying the GCE substrate, the GCE was treated with 0.05 μm alumina slurry and rinsed by ultrasonic cleaning with ethanol and deionized water for 5 min, respectively. Then, 1 mg sample of **1** was dispersed into 1 mL ethanol and treated by ultrasonication for 30 min to form a homogeneous suspension. Each time before electrode was modified by suspension, ultrasonic treatment for another 30 min was needed. Afterwards, the suspension (5 μL) and Nafion solution (2 μL , 1%) were successively dripping on the GCE surface based on electrostatic interactions to obtain the Mn(II)-based CPs modified electrode (**1**/GCE). Through a similar method, Ag@**1**-modified electrode (Ag@**1**/GCE) was obtained, which was dried at room temperature before further measurement.

1.4 Characterization and electrochemical test

Scanning electron microscopy (SEM, Hitachi S-4800, Japan) was used to observe the hybrid morphology at the voltage of 2 kV. IR spectra were acquired as KBr discs using a Bruker EQUINOX-55 FT-IR spectrometer varying from 400 to 4 000 cm^{-1} . X-ray photoelectron spectra (XPS, ESCALAB 250xi) and powder X-ray diffraction measurements (PXRD, Bruker D8 ADVANCE) were used to observe the chemical composition and structure of the obtained sample. X-ray diffractometer employing Cu $K\alpha$ radiation ($\lambda=0.154\ 18\ \text{nm}$) within a 2θ range of 5° - 50° . Moreover, the operating voltage and current are 40 kV and 40 mA, respectively. Thermogravimetric analyses (TGA) curves were collected with a NETZSCH STA 449 CTG/DTA equipment under N_2 stream at a heating rate of $10\ \text{C}\cdot\text{min}^{-1}$. Electrochemical measurements were conducted on the electrochemical workstation (IVIUM Vertax) with a three-electrode configuration containing a working electrode of a modified GCE ($\Phi=3\ \text{mm}$), a reference electrode of Ag/AgCl ($3\ \text{mol}\cdot\text{L}^{-1}\ \text{KCl}$) and a counter

electrode of platinum wire ($0.5\ \text{mm}\times 37\ \text{mm}$).

All the cyclic voltammetry (CV) curves were collected in $0.1\ \text{mol}\cdot\text{L}^{-1}\ \text{NaOH}$ aqueous electrolyte with and without glucose ($1\ \text{mmol}\cdot\text{L}^{-1}$). Preliminary to electrochemical test, Ag@**1**/GCE was scanned ten times in electrolyte containing $0.1\ \text{mol}\cdot\text{L}^{-1}\ \text{NaOH}$ until CV curves coincided, thus activating Ag@**1**/GCE. The chronoamperometric responses of Ag@**1** electrode towards glucose were measured at the applied voltage of 0.85 V (vs Ag/AgCl), then the stability and repeatability test were carried out. During the whole process of chronoamperometric test, the electrolyte was continuously stirred by magneton and glucose was added at the same time interval of 50 s.

1.5 Crystallographic data collection and refinement

Crystallographic data for **1** was collected by using a Bruker SMART APEX II CCD diffractometer equipped with graphite monochromated Mo $K\alpha$ radiation ($\lambda=0.071\ 07\ \text{nm}$). The structure was solved by direct methods and refined on F^2 by full-matrix least-squares procedures with SHELXL program. The non-hydrogen atoms were refined anisotropically, while the hydrogen atoms were added to their geometrically ideal positions and refined isotropically. The crystallographic data and structural refinement parameters are given in Table 1, and selected bond lengths and angles are listed in Table S1 (Supporting information).

CCDC: 2080639.

2 Results and discussion

2.1 Structural description

Single crystal X-ray diffraction analysis demonstrates that complex **1** is a 2D framework. Complex **1** belongs to the tetragonal $P2_1/n$ space group. As shown in Fig. 1a, the asymmetric unit consists of one Mn(II) center, one PIAD²⁻ ligand, one DMF molecule and one free water molecule. Mn1 with a distorted octahedral coordination geometry is linked to one N atom and four O atoms from four PIAD²⁻ ligands, and one O atom from one DMF molecule. The Mn—O bond distances vary from 0.210 0(2) to 0.235 1(2) nm, and the Mn—N bond distance is 0.228 3(3) nm. The O—Mn—O

Table 1 Crystallographic data and structural refinement parameters of **1**

Parameter	1	Parameter	1
Empirical formula	C ₁₆ H ₁₆ MnN ₂ O ₆	Z	4
Formula weight	387.25	D _c / (g·cm ⁻³)	1.531
Crystal system	Monoclinic	μ / mm ⁻¹	0.821
Space group	P2 ₁ /n	Reflection collected	10 093
T / K	296.15	Reflection unique	3 949
a / nm	1.056 6(4)	R _{int}	0.049 2
b / nm	1.141 9(4)	GOF	1.038
c / nm	1.400 6(5)	R ₁ , wR ₂ [I>2σ(I)]	0.058 9, 0.159 7
β / (°)	96.276(7)	R ₁ , wR ₂ (all data)	0.080 4, 0.186 0
V / nm ³	1.679(11)		

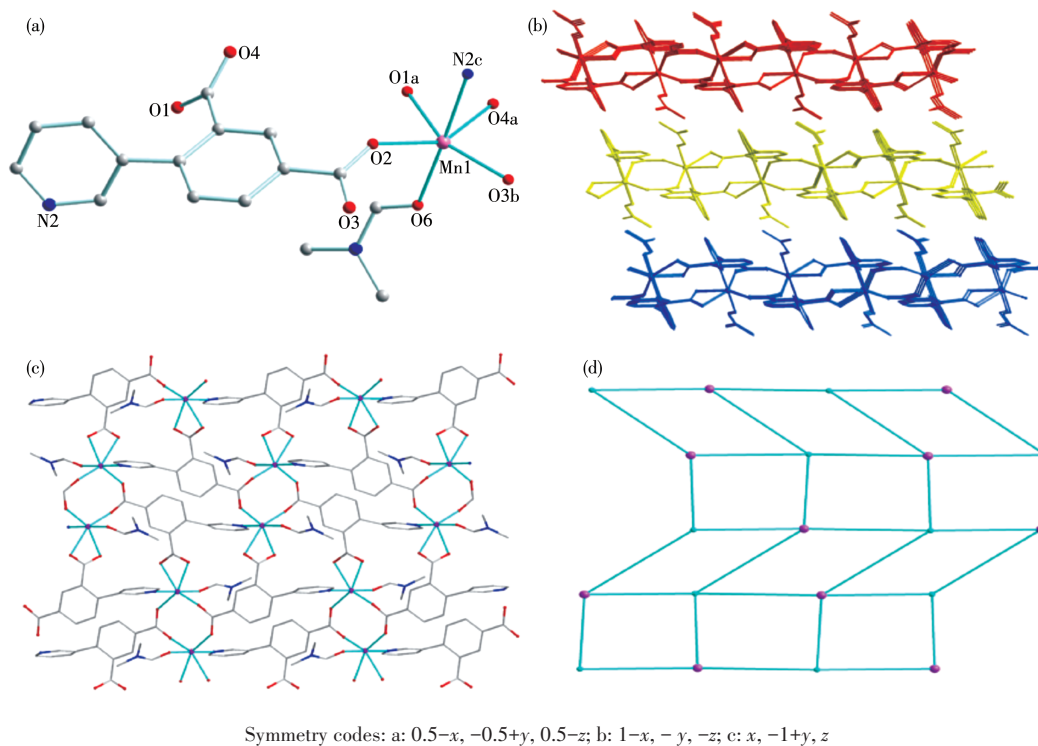


Fig.1 (a) Coordination environment of Mn(II) ion in **1**; (b) 2D layered network of **1** viewed along *a* axis; (c) 2D structure of **1** viewed along *b* axis; (d) 4,4-connected topological net of **1**, where pink nodes and blue stick represent Mn(II) ions and ligands, respectively

angles vary from 56.95(8)° to 151.30(9)°, and the N—Mn—O angles vary from 83.15(9)° to 177.87(10)°.

The carboxylate groups in PIAD²⁻ ligand adopt two coordination fashion: (κ^1 - κ^1)- μ_1 -COO⁻ and (κ^1 - κ^1)- μ_2 -COO⁻, to link Mn(II) ions and further extend to a 2D sheet (Fig. 1b and 1c). The neighboring 2D sheets are held together to construct a supramolecular 3D structure. Topologically, both Mn1 and PIAD²⁻ ligands can be simplified as 4-connected nodes. The structure of **1** represents (4, 4)-connected *sql* topological net with a

point symbol of (4⁴·6²) (Fig. 1d).

2.2 Characterizations

In this work, powder-like **1** was dispersed in the solution containing Ag⁺ precursors and then reduced by NaBH₄ to yield Ag@**1** nanocomposite. As-prepared Ag@**1** was also verified by IR, TGA, SEM, PXRD analysis. The SEM coupled with energy-dispersive X-ray spectroscopy (EDX) was used to further visualize the coverage of Ag NPs on modified matrix of **1**. As shown in Fig. 2a, most of **1** had a blocky shape with a size of

ca. 200 μm along the length. It is explained that **1**, as a matrix, provides a large surface for carrying more Ag to enhance Ag@**1** electrocatalytic activity. When Ag NPs were embedded onto **1**, as shown in Fig. 2b, Ag@**1** nanocomposite with a slightly smaller particle diameter kept the original morphology. It could be seen within the measured area from Fig. 2c that Ag@**1** comprised of the elements of C, N, O, Mn and Ag. The XPS spectra of Ag@**1** further confirmed the presence of these elements (Fig. 3). The Ag3d peaks appeared at 368.14 and 374.24 eV, further suggesting that Ag has been successfully loaded on the surface of **1**. Moreover, two Ag peaks had a slight shift to the left, respectively, which could be assigned to the metallic Ag NPs^[42]. Besides,

the structural stability of Ag@**1** was measured by TGA (Fig.S1). For Ag@**1**, the similar but not identical TGA curve also indicated the intact frameworks structure of **1**. It should be noted that the weight of the final product for Ag@**1** was higher than **1**, which was consistent with Ag NPs in composites. The IR spectrum of **1** is depicted in Fig.S2.

From the PXRD pattern of **1** (Fig. S3), all the peaks matched well with the simulated pattern of **1**, confirming the phase purity of **1**. For Ag@**1**, the diffraction peaks of **1** could be well identified, revealing its retained original structure after embedding Ag NPs onto **1**. In addition, after **1** was immersed in 0.1 mol·L⁻¹ NaOH for three days, the PXRD pattern showed

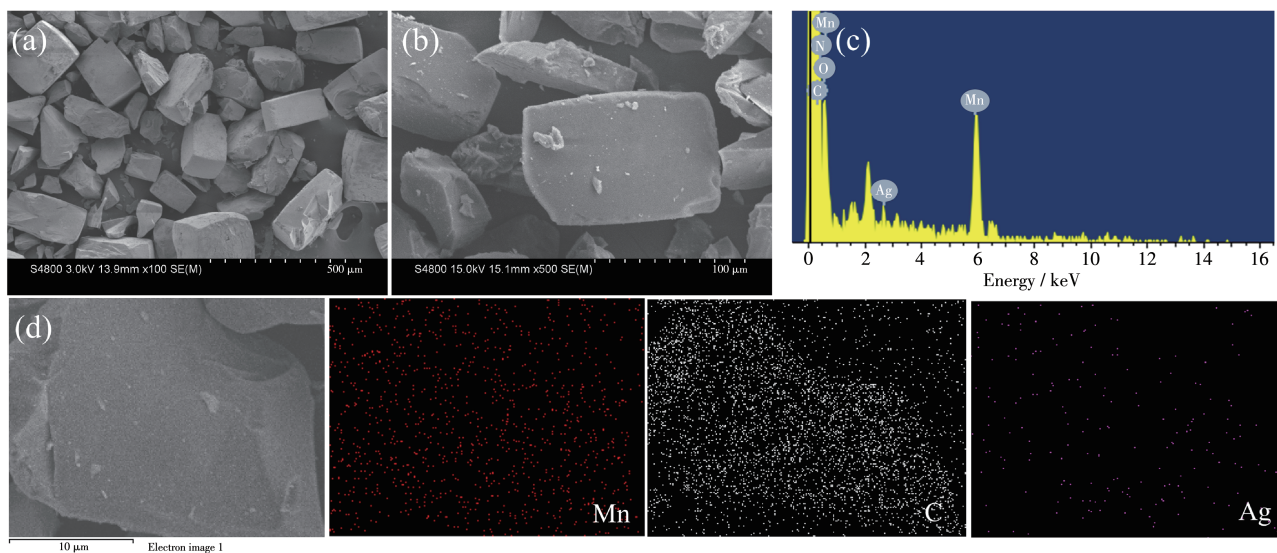


Fig.2 Morphology characterization and element analysis of Ag@**1**: SEM images of (a) **1** and (b) Ag@**1**; (c) EDX spectrum of Ag@**1**; (d) Relative composition map of Mn, Ag and C elements

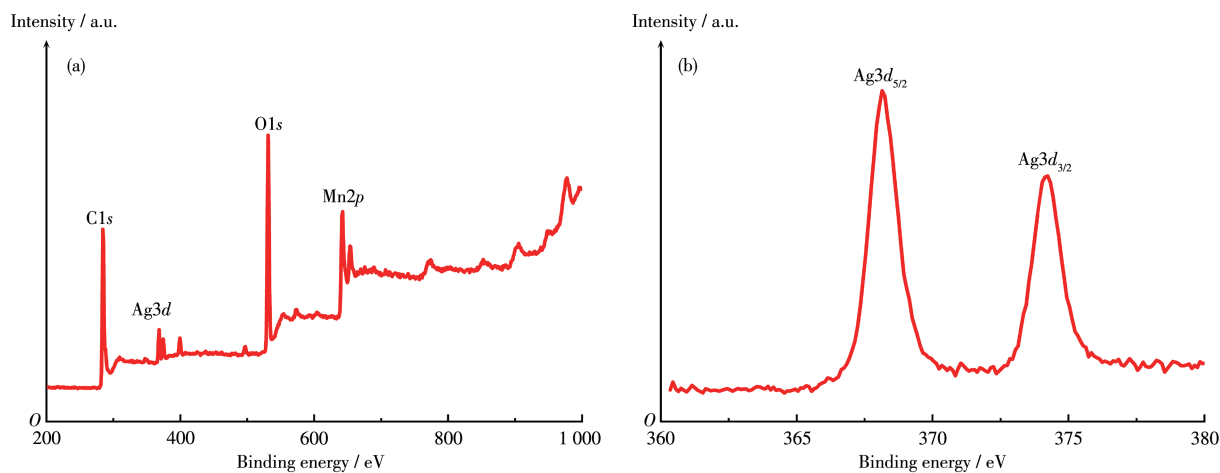


Fig.3 XPS spectra of (a) Ag@**1** and (b) Ag3d in Ag@**1**

that the structure of **1** could keep stable in $0.1 \text{ mol} \cdot \text{L}^{-1}$ NaOH. Both TGA and PXRD results corroborate successful integration hybrids of Ag NPs with **1** (Fig. S1 and Fig. S3). This gives enough evidence illustrating that Ag@**1** can be designed and constructed as a novel non-enzymatic glucose sensor.

2.3 Electrochemical sensing

Since **1** and OH^- species are involved in the electro-oxidation of the glucose, it is expected that OH^- plays a role in the catalyst process. Previous studies explored the effect of NaOH concentration on the glucose oxidation current in the literature^[43]. Hence, $0.1 \text{ mol} \cdot \text{L}^{-1}$ NaOH electrolyte was used for further electrochemical test of glucose oxidation efficiently.

The CV curves of GCE, **1**/GCE and Ag@**1**/GCE

were investigated in the absence and presence of $1 \text{ mmol} \cdot \text{L}^{-1}$ glucose with the whole potential window from -1.0 to 1.0 V . As shown in the inset of Fig. 4a, the CV curve of bare GCE did not appear as a redox peak. Meanwhile, it was found that the presence or absence of glucose did not alter the curve trails, revealing the bare GCE electrode had negligible catalytic activity for glucose oxidation. However, after the redox-active **1** was coated on the GCE, a small reduction current was received. With the addition of glucose toward **1**/GCE, the visible increase of redox peaks was observed at peak III/IV, which demonstrate the moderate electrocatalytic performance of **1** for glucose oxidation. For **1**, two pairs of asymmetric redox peaks position corresponding to the peak III/IV in the inset of Fig. 4a con-

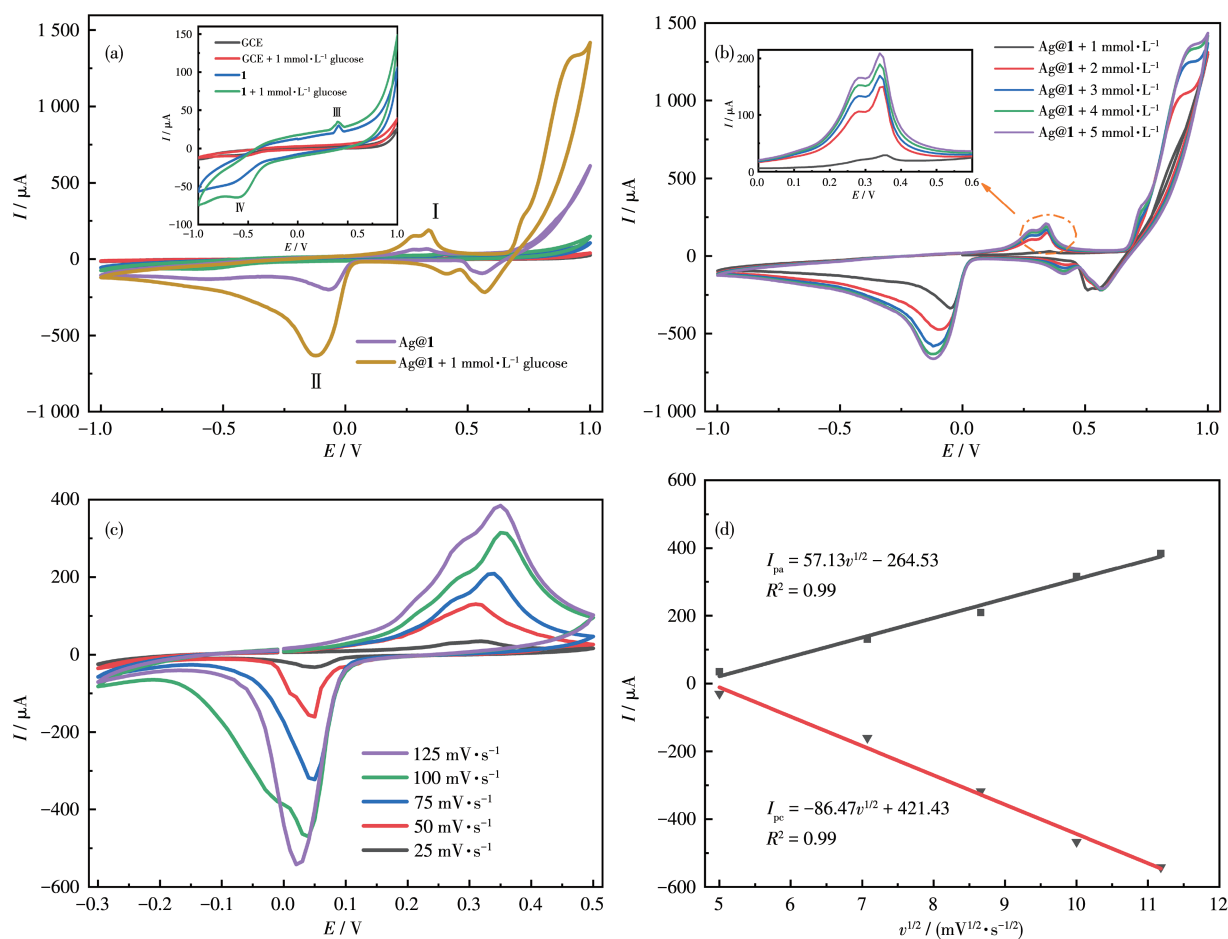
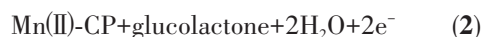
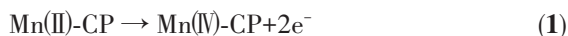


Fig. 4 (a) CV curves (Scan rate: $50 \text{ mV} \cdot \text{s}^{-1}$) of the response with and without $1 \text{ mmol} \cdot \text{L}^{-1}$ glucose in $0.10 \text{ mol} \cdot \text{L}^{-1}$ NaOH solution for Ag@**1**/GCE and GCE, **1**/GCE (Inset); (b) CV curves (Scan rate: $50 \text{ mV} \cdot \text{s}^{-1}$) of Ag@**1** electrode in $0.10 \text{ mol} \cdot \text{L}^{-1}$ NaOH solution containing 1 - $5 \text{ mmol} \cdot \text{L}^{-1}$ glucose (Inset: enlarged view of 0 - 0.6 V range); (c) CV curves of Ag@**1** electrode at different scan rates (25 , 50 , 75 , 100 and $125 \text{ mV} \cdot \text{s}^{-1}$) in $0.10 \text{ mol} \cdot \text{L}^{-1}$ NaOH solution; (d) Plots of the square root of scan rate vs peak current at anodic and cathode for Ag@**1**/GCE

firm redox activity, and could be found at around 0.41 and -0.61 V, respectively.

As shown in Fig.4a, upon adding $1 \text{ mmol} \cdot \text{L}^{-1}$ glucose, for peak I, Ag@1/GCE exhibited a much higher anodic current in the presence of glucose than that in the absence of glucose. The highest anode peak current showed that the introduction of Ag NPs significantly improved catalytic activity of 1 as catalyst, which guaranteed that Ag@1/GCE had better performance as a glucose sensor. And the possible redox reactions for glucose on the surface of Ag@1/GCE could be assigned to the reversible transition in the oxidation state between Mn(II) and Mn(IV) ions^[44-46]. First, the Mn(II) center would be oxidized to Mn(IV). Then the oxidative Mn could catalyze glucose oxidation to generate gluconolactone^[47-48].



Besides, the distinctive feature of CV curves between 1/GCE and Ag@1/GCE appeared in a few aspects: the position of current start rising for Ag@1/GCE shifted to around 0.05 V (vs Ag/AgCl); the potentials of the anodic peak for Ag@1/GCE centered at 0.34 V (vs Ag/AgCl), lower than 1/GCE electrode at 0.41 V; the current responses for both 1/GCE and Ag@1/GCE gave a soared current signal to ensure both the electrodes can catalyze the electrochemical oxidation of glucose. The catalytic mechanism process of Ag@1/GCE is shown in Fig.5.

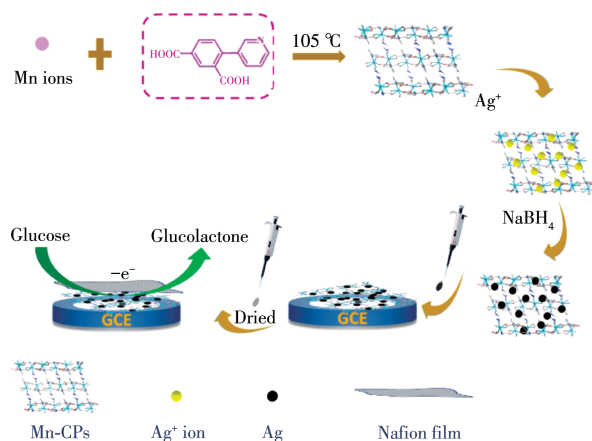


Fig.5 Catalytic mechanism process of Ag@1/GCE for glucose oxidation

To further investigate the ability of Ag@1 to catalyze and oxidize glucose under alkaline conditions, the CV curves of Ag@1 in the presence of glucose with different concentrations (1.0 – $5.0 \text{ mmol} \cdot \text{L}^{-1}$) were tested subsequently with an electrolyte solution containing $0.1 \text{ mol} \cdot \text{L}^{-1}$ NaOH (Fig.4b). With the increase of the glucose concentration, an increasing trend can be observed in the anode peak (II) current (up to $200 \mu\text{A}$). Meanwhile, the oxidation peak potential shifted slightly positively with the increasing glucose concentration, indicating that Ag@1 has excellent catalytic oxidation ability for glucose.

Furthermore, the CV curves at various scan rates were collected for Ag@1/GCE (Fig.4c). Notably, as scan rate increased from 25 to $125 \text{ mV} \cdot \text{s}^{-1}$, the potentials of anodic peaks (I) and cathodic peaks (II) become higher and lower, respectively, which can be related to the electrochemical relaxation phenomenon. Besides, as shown in Fig.4d, the currents at anodic (I_{pa} , μA) and cathodic (I_{pc} , μA) peaks for Ag@1/GCE were directly proportional with the square root of the scan rate ($v^{1/2}$), which proves out that the electrochemical process of Ag@1 toward glucose oxidation is diffusion-controlled^[49].

2.4 Optimization for sensor ability of Ag@1

Working potential is an indispensable factor for optimization performance of a sensor. Through continuous injection of $1.0 \text{ mmol} \cdot \text{L}^{-1}$ glucose, the current response under three voltages of 0.8, 0.85 and 0.9 V was studied, so as to optimize the sensing ability of Ag@1. As depicted in Fig.S4, the three applied potentials exhibited similar current response trend. Meanwhile, the current signal for 0.8 V was so weak that it increased the error in the quantitative calculation of glucose concentration. The potential at 0.9 V was not conducive to the sensitivity of Ag@1 sensor. Therefore, the potential of 0.85 V had relatively less influence on the currents compared with 0.9 V, and a potential of 0.85 V was used for the I - t curve test. As shown in Fig.6a, the consecutive step changes after each glucose injection in I - t plot revealed that the glucose response signal was positively correlated with glucose concentration and the current signal reached its steady-state value (95% of the maximum) within 6 s. The calibra-

tion curve (Fig. 6b) showed the linear relationship between the current signal (I , μA) and glucose concentration (c , $\text{mmol}\cdot\text{L}^{-1}$) in a range of 10-4 540 $\mu\text{mol}\cdot\text{L}^{-1}$, which can be expressed by a linear equation: $I=11.67c+5.21$ ($R^2=0.99$). The sensitivity was calculated to be $166.71 \mu\text{A}\cdot\text{L}\cdot\text{mmol}^{-1}\cdot\text{cm}^{-2}$, and a low detection limit (LOD) of $6.36 \mu\text{mol}\cdot\text{L}^{-1}$ was found based on the signal-to-noise ratio of 3 for Ag@1/GCE sensor. A comparison of the analytical performance for this Mn(II)-based CPs with other non-enzymatic glucose sensors is shown in Table 2. In this work, the combination of Ag NPs and CPs to form Ag@1 composites can reduce the oxidation

potential of glucose oxidation and improved its catalytic ability. Ag@1 sensor was offered to have a wide linear dynamic range and high sensitivity for glucose detection. It is conjectured that Ag@1/GCE well-performance arises from the following reasons: (i) the Mn(II)-based CPs as supporting structure offers a platform; (ii) the excellent electronic conductivity of Ag NPs and Nafion film could provide reliable interaction towards the glucose molecules; (iii) the presence of metal active sites of Mn-CPs enables large amounts of glucose molecules on the surface of Ag@1/GCE for efficient oxidation.

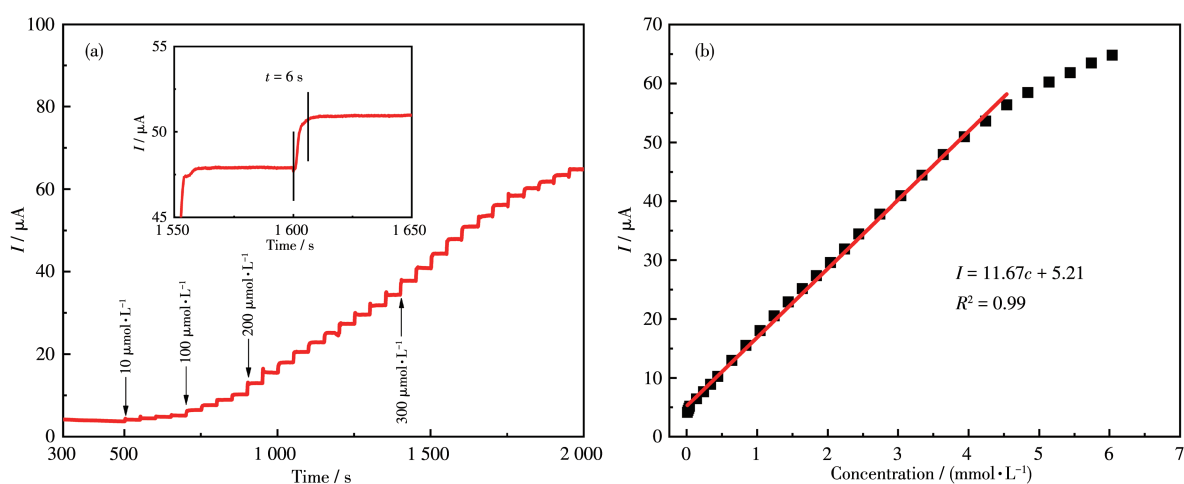


Fig. 6 (a) I - t curve of Ag@1/GCE by continuously addition of glucose in $0.1 \text{ mol}\cdot\text{L}^{-1}$ NaOH electrolyte at an applied potential of 0.85 V (vs Ag/AgCl); (b) Calibration curve between glucose concentration and its current signal for Ag@1/GCE at 0.85 V (vs Ag/AgCl)

Table 2 Comparison of electrocatalytic abilities between Ag@1/GCE and other non-enzymatic sensors

Modified electrode	Linear range / ($\mu\text{mol}\cdot\text{L}^{-1}$)	Sensitivity / ($\mu\text{A}\cdot\text{L}\cdot\text{mmol}^{-1}\cdot\text{cm}^{-2}$)	LOD / ($\mu\text{mol}\cdot\text{L}^{-1}$)	Ref.
MnO _x -30/Au	7-10 600	811.8 ($\mu\text{A}\cdot\text{L}\cdot\text{mmol}^{-1}$)	2.7	[50]
Cu ₇ S ₄ hollow nanospheres	1.0-2 000	3 728.7	0.023	[51]
Cu ₂ ZnSnS ₄ quantum dot	0.5-2 000	2 503	0.013	[52]
Mn ₃ O ₄ /3DCGF	100-8 000	360	10	[53]
Ag@TiO ₂ @ZIF-67	48-1 000	0.788	0.99	[54]
Ag@1/GCE	10-4 540	166.71	6.36	This work

2.5 Selectivity, stability and repeatability of Ag@1 sensor

The anti-interference performance is also an essential condition for a glucose sensor. The specificity of Ag@1 sensor was investigated by the chronoamperometry response to the interferences. The interfering substances, such as uric acid (UA), ascorbic acid

(AA), sucrose, lactose, galactose, fructose, usually coexist with glucose inevitably in human serum, and their concentrations are less than 30 times that of glucose. Fig. 7a depicts the response curve of Ag@1/GCE to continuous addition of $1 \text{ mmol}\cdot\text{L}^{-1}$ glucose and $0.1 \text{ mmol}\cdot\text{L}^{-1}$ interference species. When $1 \text{ mmol}\cdot\text{L}^{-1}$ glucose was firstly added, a significantly rising current

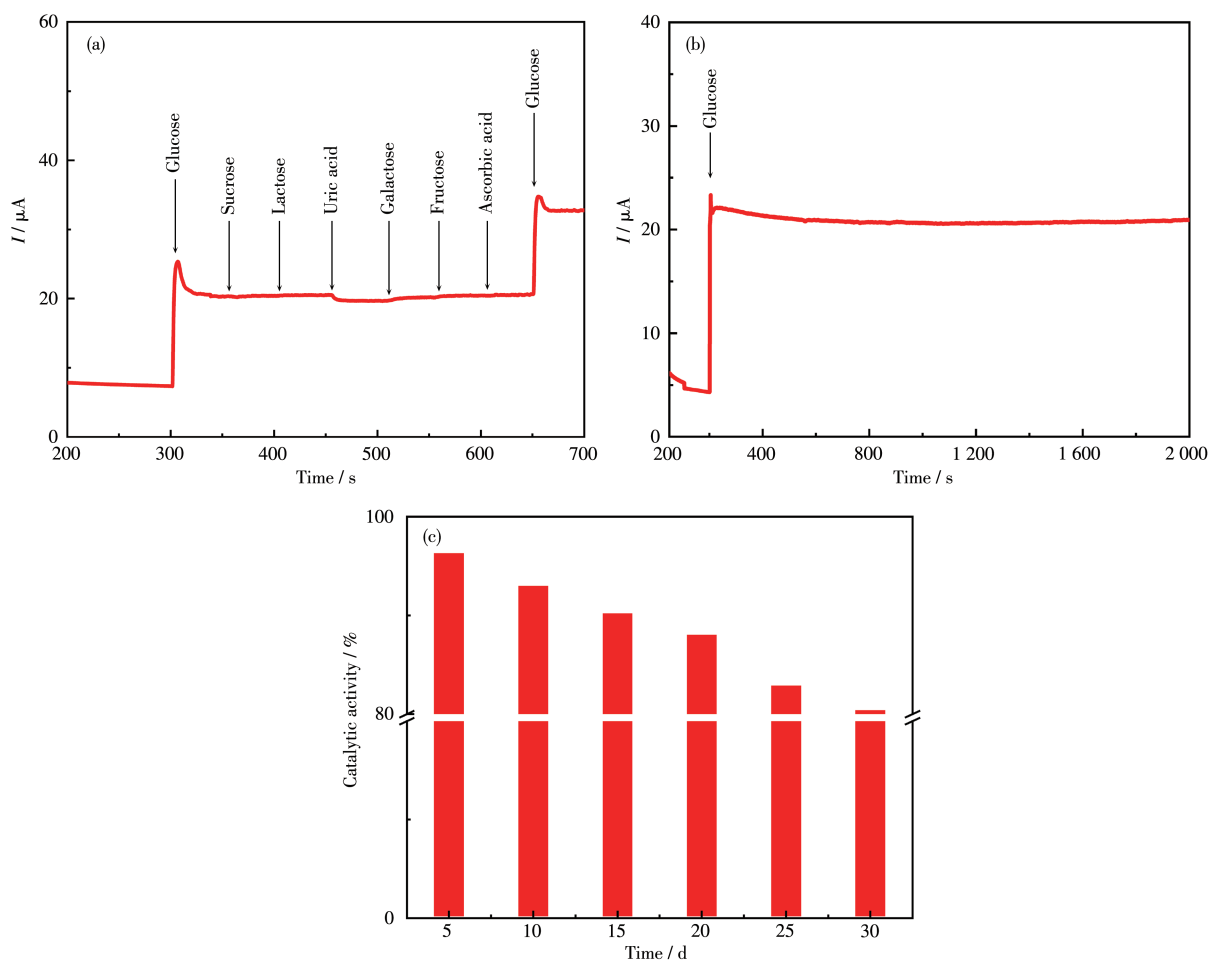


Fig.7 (a) $I-t$ curve of Ag@1/GCE with successive addition of $1 \text{ mmol} \cdot \text{L}^{-1}$ glucose and other $0.1 \text{ mmol} \cdot \text{L}^{-1}$ interfering species; (b) Stability of Ag@1/GCE to $1 \text{ mmol} \cdot \text{L}^{-1}$ glucose in $0.1 \text{ mol} \cdot \text{L}^{-1}$ NaOH solution at 0.85 V for $2\ 000 \text{ s}$; (c) Changes of catalytic activity of the same Ag@1/GCE during 30 d of storage time

response was observed, and the other kinds of interferences caused the negligible current response. After adding $1 \text{ mmol} \cdot \text{L}^{-1}$ glucose again, the current signal was the same as when adding glucose for the first time. These results indicated that Ag@1 sensor had excellent selectivity for the detection of glucose.

In addition, the long-term stability of this optimized sensor was also examined. As shown in Fig.7b, the current signal appeared tiny descend for a long period of $2\ 000 \text{ s}$. Moreover, Ag@1/GCE was stored for stability analysis as displayed in Fig.7c, and its activity was tested every 5 d . It should be noted that after Ag@1/GCE was stored for 10 d , the activity decreased by 6.85% , and it remained at the original 80.6% after 30 d . The good stability is due to the presence of Nafion film which significantly slowed down the peel of com-

posite film from Ag@1/GCE surface, thus further manifested the stability and recyclable electrocatalytic activity of Ag@1. As to the repeatability test, through recording the five sets of mean values of the current changes of the parallel samples on Ag@1/GCE, the relative standard deviation (RSD) was calculated to be 5.34% (Fig.S5).

3 Conclusions

In summary, a novel CP structure (1) with a PIAD²⁻ ligand has been successfully synthesized firstly for the non-enzymatic sensor of glucose in a facile way. Here, the containing-Ag@1 suspension was adsorbed on the electrode surface directly, then the Nafion solution was coated on the GCE surface and efficiently restrained the CPs fall-off. The as-prepared low-cost

glucose sensor based on Ag@**1** exhibited good sensitivity, selectivity and stability. More interestingly, for Ag@**1**, the interference from the oxidation of common six interfering species such as AA and UA was effectively avoided. It is found that the Mn(II)-based CPs can be used as immobilization hosts to load NPs in the glucose electrocatalysis. Furthermore, this research has great significance for exploring the application in electrocatalysis with poorly conductivity CPs as a catalytic active center and also provides a promising idea for the development of non-enzymatic electrochemical sensors.

Supporting information is available at <http://www.wjhxsb.cn>

References:

- [1] Shibayama T, Tanha S, Abe Y, Haginoya H, Rajab A, Hidaka K. The Role of Illness Schemata in Self - Care Behaviors and Glycemic Control among Patients with Type 2 Diabetes in Iran. *Prim. Care Diabetes*, **2019**,**13**(5):474-480
- [2] Ferri S, Kojima K, Sode K. Review of Glucose Oxidases and Glucose Dehydrogenases: A Bird's Eye View of Glucose Sensing Enzymes. *J. Diabetes Sci. Technol.*, **2011**,**5**(5):1068-1076
- [3] Vashist S K, Zheng D, Al-Rubeaan K, Luong J H T, Sheu F S. Technology behind Commercial Devices for Blood Glucose Monitoring in Diabetes Management: A Review. *Anal. Chim. Acta*, **2011**,**703**(2):124-136
- [4] Zhang Y, Zheng D H, Liu S M, Qin S Y, Sun X H, Wang Z F, Qin C L, Li Y Y, Zhou J. Flexible Porous Ni(OH)₂ Nanopetals Sandwiches for Wearable Non - enzyme Glucose Sensors. *Appl. Surf. Sci.*, **2021**, **552**:149529
- [5] Zhang J, Sun Y D, Li X C, Xu J S. Fabrication of NiCo₂O₄ Nanobelt by a Chemical Co - precipitation Method for Non - enzymatic Glucose Electrochemical Sensor Application. *J. Alloys Compd.*, **2020**, **831**: 154796
- [6] Li W W, Qi H, Wang B G, Wang Q Y, Wei S T, Zhang X L, Wang Y, Zhang L, Cui X Q. Ultrathin NiCo₂O₄ Nanowalls Supported on a 3D Nanoporous Gold Coated Needle for Non - enzymatic Amperometric Sensing of Glucose. *Mikrochim. Acta*, **2018**,**185**(2):124
- [7] Lee S, Lee J, Park S, Boo H, Kim H C, Chung T D. Disposable Non - enzymatic Blood Glucose Sensing Strip Based on Nanoporous Platinum Particles. *Appl. Mater. Today*, **2018**,**10**:24-29
- [8] Liu B B, Wang X Y, Liu H Q, Zhai Y Y, Li L, Wen H R. 2D MOF with Electrochemical Exfoliated Graphene for Nonenzymatic Glucose Sensing: Central Metal Sites and Oxidation Potentials. *Anal. Chim. Acta*, **2020**,**1122**:9-19
- [9] Nantaphol S, Watanabe T, Nomura N, Siangproh W, Chailapakul O, Einaga Y. Bimetallic Pt - Au Nanocatalysts Electrochemically Deposited on Boron-Doped Diamond Electrodes for Nonenzymatic Glucose Detection. *Biosens. Bioelectron.*, **2017**,**98**:9876-9882
- [10] Hwang D W, Lee S, Seo M, Dong C T. Recent Advances in Electrochemical Non - enzymatic Glucose Sensors-A Review. *Anal. Chim. Acta*, **2018**,**1033**:1-34
- [11] Liu T J, Guo Y Q, Zhang Z F, Miao Z C, Zhang X Y, Su Z Q. Fabrication of Hollow CuO/PANI Hybrid Nanofibers for Non-enzymatic Electrochemical Detection of H₂O₂ and Glucose. *Sens. Actuators B*, **2019**, **286**:370-376
- [12] Hu M L, Abbasi-Azad M, Habibi B, Rouhani F, Moghanni-Bavil-Olyaei H, Liu K G, Morsali A. Electrochemical Applications of Ferrocene-Based Coordination Polymers. *ChemPlusChem*, **2020**, **85**(11): 2397-2418
- [13] Liu G C, Zhao J, Liang S, Li Y, Chang Z H, Wang X L, Chen B K. Ten Polytorsional-Amide-Induced Helical-Based Coordination Polymers with Difunctional Electrochemical Activities. *CrystEngComm*, **2021**,**23**(5):1263-1271
- [14] Zhao Q, Li S H, Chai R L, Ren X, Zhang C. Two-Dimensional Conductive Metal - Organic Frameworks Based on Truxene. *ACS Appl. Mater. Interfaces*, **2020**,**12**(6):7504-7509
- [15] Yang M L, Rong S, Wang X M, Ma H Y, Pang H J, Tan L C, Jiang Y X, Gao K Q. Preparation and Application of Keggin Polyoxometalate-Based 3D Coordination Polymer Materials as Supercapacitors and Amperometric Sensors. *ChemNanoMat*, **2021**,**7**(3):299-306
- [16] Wang Y, Wang L, Huang W, Zhang T, Hu X Y, Perman J A, Ma S Q. A Metal-Organic Framework and Conducting Polymer Based Electrochemical Sensor for High Performance Cadmium Ion Detection. *J. Mater. Chem. A*, **2017**,**5**(18):8385-8393
- [17] Tang L P, Yang S, Liu D, Wang C, Ge Y Q, Tang L M, Zhou R L, Zhang H. Two-Dimensional Porous Coordination Polymers and Nanocomposites for Electrocatalysis and Electrically Conductive Applications. *J. Mater. Chem. A*, **2020**,**8**(29):14356-14383
- [18] Zhang X, Zhao K X, Lin S Y, Xu Z K, Li L. Ambient Synthesis of Iron-Nickel Amorphous Coordination Polymer Nanosheet Arrays for Highly Efficient Oxygen Evolution Electrocatalysis. *J. Alloys Compd.*, **2021**,**868**:159218
- [19] Allendorf M D, Bauer C A, Bhakta R K, Houk R J T. Luminescent Metal-Organic Frameworks. *Chem. Soc. Rev.*, **2009**,**38**(5):1330-1352
- [20] Ling Y Y, Chen H M, Zhou J J, Tao K S, Zhao H, Yu X B, Han L. Metal - Organosulfide Coordination Polymer Nanosheet Array as a Battery - Type Electrode for an Asymmetric Supercapacitor. *Inorg. Chem.*, **2020**,**59**(10):7360-7369
- [21] Fu D C, Chen Z Y, Yu C Y, Song X L, Zhong W B. Bimetallic-Organic Coordination Polymers to Prepare N - Doped Hierarchical Porous Carbon for High Performance Supercapacitors. *Prog. Nat. Sci.*, **2019**, **29**(5):495-503
- [22] Wang G N, Chen T T, Gómez-García C, Zhang F, Zhang M Y, Ma H Y, Pang H J, Wang X M, Tan L C. A High-Capacity Negative Electrode for Asymmetric Supercapacitors Based on a PMo₁₂ Coordination Polymer with Novel Water - Assisted Proton Channels. *Small*, **2020**,**16**(29):2001626

- [23]Kadirov M K, Minzanova S T, Nizameev I R, Mironova L G, Gilmudinov I F, Khrizanforov M N, Kholin K V, Khamatgalimov A R, Semyonov V A, Morozov V I, Kadirov D M, Mukhametzhanov A R, Budnikova Y H, Sinyashin O G. Correction: A Nickel-Based Pectin Coordination Polymer as an Oxygen Reduction Reaction Catalyst for Proton-Exchange Membrane Fuel Cells. *Inorg. Chem. Front.*, **2019**,**6**(1):326-326
- [24]李江, 韩森, 陈团结, 苟召曦, 张琪, 聂晓双, 曹海茹. 两个金属有机框架化合物对硝基芳香化合物在气/液相的荧光传感. *无机化学学报*, **2019**,**35**(10):1843-1852
- LI J, HAN S, CHEN T J, GOU Z X, ZHANG Q, NIE X S, CAO H R. Two Homologous Metal-Organic Frameworks Based on Zn(II) and Cd(II): Luminescent Sensors for Nitro Aromatic Compounds in Solution and Vapor Medium. *Chinese J. Inorg. Chem.*, **2019**,**35**(10):1843-1852
- [25]Shahhoseini L, Mohammadi R, Ghanbari B, Shahrokhian S. Ni(II) 1D-Coordination Polymer/C₆₀-Modified Glassy Carbon Electrode as a Highly Sensitive Non-enzymatic Glucose Electrochemical Sensor. *Appl. Surf. Sci.*, **2019**,**478**:361-372
- [26]Liu H, Wang Y S, Qin Z S, Liu D, Xu H, Dong H L, Hu W P. Electrically Conductive Coordination Polymers for Electronic and Optoelectronic Device Applications. *J. Phys. Chem. Lett.*, **2021**,**12**(6):1612-1630
- [27]Mo G Q, Zheng X R, Ye N B, Ruan Z X. Nitrogen-Doped Carbon Dodecahedron Embedded with Cobalt Nanoparticles for the Direct Electro-oxidation of Glucose and Efficient Nonenzymatic Glucose Sensing. *Talanta*, **2020**,**225**:121954
- [28]Li M, Dong P, Zhang Y J. Facile Design and Synthesis of Ultrafine FeCo Nanocrystallines Coupled with Porous Carbon Nanosheets as High Efficiency Non-enzymatic Glucose Sensor. *J. Alloys Compd.*, **2019**,**810**:151927
- [29]Qian C C, Han K Y, Weng W M, Zhang Y J, Ma W, Song Y H, Wang L. Electrochemical Glucose Sensor Based on Microporous Carbon/CuO@Carbon/AuNPs Integrated Electrode. *ChemistrySelect*, **2019**,**4**(19):5633-5640
- [30]Li W W, Lv S, Wang Y, Zhang L, Cui X Q. Nanoporous Gold Induced Vertically Standing 2D NiCo Bimetal-Organic Framework Nanosheets for Non-enzymatic Glucose Biosensing. *Sens. Actuators B*, **2018**,**281**:652-658
- [31]Li G F, Chen D, Chen Y J, Dong L F. MOF Ni-BTC Derived Ni/C/Graphene Composite for Highly Sensitive Non-enzymatic Electrochemical Glucose Detection. *ECS J. Solid State Sci. Technol.*, **2020**,**9**(12):121014
- [32]Shi L B, Zhu X, Liu T T, Zhao H L, Lan M B. Encapsulating Cu Nanoparticles into Metal-Organic Frameworks for Nonenzymatic Glucose Sensing. *Sens. Actuators B*, **2016**,**227**:583-590
- [33]Zheng W R, Hu L S, Lee L Y S, Wong K Y. Copper Nanoparticles/Polyaniline/Graphene Composite as a Highly Sensitive Electrochemical Glucose Sensor. *J. Electroanal. Chem.*, **2016**,**781**:155-160
- [34]Shishegari N, Sabahi A, Manteghi F, Ghaffarinejad A, Tehrani Z. Non-enzymatic Sensor Based on Nitrogen-Doped Graphene Modified with Pd Nano-Particles and NiAl Layered Double Hydroxide for Glucose Determination in Blood. *J. Electroanal. Chem.*, **2020**,**871**:114285
- [35]Shabnam L, Faisal S N, Roy A K, Haque E, Minett A I, Gomes V G. Doped Graphene/Cu Nanocomposite: A High Sensitivity Non-enzymatic Glucose Sensor for Food. *Food Chem.*, **2017**,**221**:751-759
- [36]Khosroshahi Z, Karimzadeh F, Kharaziha M, Allafchian A. A Non-enzymatic Sensor Based on Three-Dimensional Graphene Foam Decorated with Cu-xCu₂O Nanoparticles for Electrochemical Detection of Glucose and Its Application in Human Serum. *Mater. Sci. Eng. C*, **2020**,**108**:110216
- [37]Chang G, Shu H H, Huang Q W, Oyama M, Ji K, Liu X, He Y B. Synthesis of Highly Dispersed Pt Nanoclusters Anchored Graphene Composites and Their Application for Non-enzymatic Glucose Sensing. *Electrochim. Acta*, **2015**,**157**:149-157
- [38]Chen C Y, Shi M, Xue M W, Hu Y J. Synthesis of Nickel(II) Coordination Polymers and Conversion into Porous NiO Nanorods with Excellent Electrocatalytic Performance for Glucose Detection. *RSC Adv.*, **2017**,**7**(36):22208-22214
- [39]Dang W J, Sun Y M, Jiao H, Xu L, Lin M. AuNPs-NH₂/Cu-MOF Modified Glassy Carbon Electrode as Enzyme-Free Electrochemical Sensor Detecting H₂O₂. *J. Electroanal. Chem.*, **2020**,**856**:113592
- [40]Razmi H, Shirdel H, Rezaei R M. NiO Nanoparticles Electrodeposited on Reduced GO-CuO Nanocomposite Bulk Modified CCE as a Sensitive Glucose Sensor. *Micro Nano Lett.*, **2017**,**12**(4):217-222
- [41]Liu Y, Shi W J, Lu Y K, Liu G, Hou L, Wang Y Y. Nonenzymatic Glucose Sensing and Magnetic Property Based on the Composite Formed by Encapsulating Ag Nanoparticles in Cluster-Based Co-MOF. *Inorg. Chem.*, **2019**,**58**(24):16743-16751
- [42]Jiang H L, Akita T, Ishida T, Haruta M, Xu Q. Synergistic Catalysis of Au@Ag Core-Shell Nanoparticles Stabilized on Metal-Organic Framework. *J. Am. Chem. Soc.*, **2011**,**133**(5):1304-1306
- [43]Meng W, Wen Y Y, Dai L, He Z X, Wang L. A Novel Electrochemical Sensor for Glucose Detection Based on Ag@ZIF-67 Nanocomposite. *Sens. Actuators B*, **2018**,**260**:852-860
- [44]Kubota R, Takabe T G, Arima K, Taniguchi H, Asayama S, Kawakami H. New Class of Artificial Enzyme Composed of Mn-Porphyrin, Imidazole, and Cucurbit[10]uril toward Use as a Therapeutic Antioxidant. *J. Mater. Chem. B*, **2018**,**6**(43):7050-7059
- [45]Sebarchievici L, Lascu A, Fagadar-Cosma G, Palade A, Fringu L, Birdeanu M, Taranu B, Fagadar-Cosma E. Optical and Electrochemical-Mediated Detection of Ascorbic Acid Using Manganese Porphyrin and Its Gold Hybrids. *C.R. Chim.*, **2018**,**21**(3/4):327-338
- [46]Chen Y L, Huang W, Wang C D, Zhai X Y, Zhang T, Wang Y, Hu X Y. Direct Growth of Poly-Glutamic Acid Film on Peroxidase Mimicking PCN-222(Mn) for Constructing a Novel Sensitive Nonenzymatic Electrochemical Hydrogen Peroxide Biosensor. *ACS Sustainable Chem. Eng.*, **2020**,**8**(35):13226-13235
- [47]Zahan M, Podder J. Role of Fe Doping on Structural and Electrical Properties of MnO₂ Nanostructured Thin Films for Glucose Sensing Performance. *Mater. Sci. Semicond. Process.*, **2020**,**117**:105109
- [48]Qu L L, Zhao L, Chen T D, Li J, Nie X S, Li R Y, Sun C J. Two Nov-

- el Coordination Polymers and Their Hybrid Materials with Ag Nanoparticles for Non-enzymatic Detection of Glucose. *J. Solid State Chem.*, **2021**,**297**:122086
- [49]Dong C Q, Zhong H, Kou T Y, Frenzel J, Eggeler G, Zhang Z H. Three-Dimensional Cu Foam-Supported Single Crystalline Mesoporous Cu₂O Nanorod Arrays for Ultra-Highly Sensitive and Efficient Nonenzymatic Detection of Glucose. *ACS Appl. Mater. Interfaces*, **2015**,**7**(36):20215-20223
- [50]Lee S H, Yang J, Han Y J, Cho M, Lee Y. Rapid and Highly Sensitive MnO_x Nanorods Array Platform for a Glucose Analysis. *Sens. Actuators B*, **2015**,**218**:137-144
- [51]Cao M M, Wang H, Kannan P, Ji S, Wang X P, Zhao Q, Linkov V, Wang R F. Highly Efficient Non-enzymatic Glucose Sensor Based on Cu₂S Hollow Nanospheres. *Appl. Surf. Sci.*, **2019**,**492**:407-416
- [52]Zhou X, Gu X T, Chen Z Y, Wu Y X, Xu W, Bao J. A Novel and Sensitive Cu₂ZnSnS₄ Quantum Dot-Based Non-enzymatic Glucose Sensor. *Sens. Actuators B*, **2021**,**329**:129117
- [53]Si P, Dong X C, Chen P, Kim D H. A Hierarchically Structured Composite of Mn₃O₄/3D Graphene Foam for Flexible Nonenzymatic Biosensors. *J. Mater. Chem. B*, **2013**,**1**:110-115
- [54]Arif D, Hussain Z, Sohail M, Liaqat M A, Khan M A, Noor T. A Non-enzymatic Electrochemical Sensor for Glucose Detection Based on Ag@TiO₂@Metal-Organic Framework (ZIF-67) Nanocomposite. *Front. Chem.*, **2020**,**8**:573510